Zfp64 participates in Notch signaling and regulates differentiation in mesenchymal cells

Kei Sakamoto*, Yoshihiro Tamamura, Ken-ichi Katsube and Akira Yamaguchi

Section of Oral Pathology, Graduate School, Tokyo Medical and Dental University, 1-5-45 Yushima, Bunkyo-ku, Tokyo 113-8549, Japan
*Author for correspondence (e-mail: s-kei.mpa@tmd.ac.jp)

Accepted 1 March 2008
Journal of Cell Science 121, 1613-1623 Published by The Company of Biologists 2008
doi:10.1242/jcs.023119

Summary

Notch signaling is required for multiple aspects of tissue and cell differentiation. In this study, we identified zinc finger protein 64 (Zfp64) as a novel coactivator of Notch1. Zfp64 is associated with the intracellular domain of Notch1, recruited to the promoters of the Notch target genes *Hes1* and *Hey1*, and transactivates them. *Zfp64* expression is under the control of Runx2, and is upregulated by direct transactivation of its promoter. Zfp64 suppresses the myogenic differentiation of C2C12 cells and promotes their osteoblastic differentiation. Our data demonstrate two functions of *Zfp64*: (1) it is a downstream target of Runx2 and, (2) its cognate protein acts as a coactivator of Notch1, which suggests that Zfp64 mediates mesenchymal cell differentiation by modulating Notch signaling.

Supplementary material available online at
http://jcs.biologists.org/cgi/content/full/121/10/1623/DC1

Key words: Notch, Runx2, Zinc finger protein 64

Introduction

Skeletal tissue is composed of many types of mesenchymal cells, which originate from common pluripotent progenitor cells. Various signaling molecules participate in directing these cells to specific differentiation pathways. Among these, bone morphogenic protein (BMP) has a crucial role in the regulation of myogenic and osteogenic lineage cells, inhibiting myogenic differentiation and promoting osteogenic differentiation (Katagiri et al., 1994). During the regulatory processes of osteoblast differentiation, BMP2 induces the expression of the runt-domain transcription factor 2 (Runx2), which is essential in regulating the expression of osteoblast-related genes, such as those for alkaline phosphatase (ALP), type I collagen, osteopontin and osteocalcin (Ducy, 2000; Komori, 2005). This major signaling cascade in osteogenesis is modified by other signaling pathways, including hedgehog, Wnt and Notch signaling (Komori, 2005; Lee et al., 2006; Nobta et al., 2005).

Notch signaling is a developmentally conserved cell-to-cell communication mechanism that regulates the differentiation of diverse tissues and cell types. Notch signaling exerts diverse effects on cell differentiation, acting to maintain stem cells in an undifferentiated state, but also promoting terminal differentiation (Wilson and Radtke, 2006). Reflecting its complex nature, contradictory data on the role of Notch signaling in osteoblast differentiation have been reported, in which Notch signaling either inhibits (Deregowski et al., 2006; Sciaudone et al., 2003; Shindo et al., 2003) or promotes osteoblastic cell differentiation (Nobta et al., 2005; Tezuka et al., 2002). The multiplicity of the Notch functions suggests the presence of complex mechanisms of signal modification and crosstalk with other signaling pathways, which have yet to be elucidated.

Notch signaling is initiated by ligand-mediated proteolytic cleavage, which facilitates the nuclear translocation of the Notch intracellular domain (NICD). The NICD forms a transcription complex with several cofactors and then activates downstream targets, such as the HES-HEY of family transcription factors. NICD consists of several distinct functional modules, including the RAM domain, ankyrin repeats, nuclear localization motifs, a transactivation domain and a PEST-containing region (Ehebauer et al., 2006). The RAM domain associates with the DNA-binding factor CSL (CBF1/Su(H)/Lag), leading to the displacement of the co-repressors and the recruitment of the coactivator protein Mastermind to the ankyrin repeats (Ehebauer et al., 2006; Fryer et al., 2004; Nam et al., 2003). The ankyrin repeats also interact with Ski-interacting protein (SKIP) (Zhou et al., 2000) or Deltex (Matsuno et al., 1998) to facilitate Notch signaling. The PEST-containing region is required for ubiquitylation by Sel-10 ubiquitin ligase and subsequent protein degradation, which mediates the rapid turnover of NICD (Gupta-Rossi et al., 2001; Oberg et al., 2001; Wu et al., 2001). The hyperphosphorylation of several conserved serine residues within this motif seems to be important for NICD ubiquitination (Fryer et al., 2004; Gupta-Rossi et al., 2001; Wu et al., 2001). In some cases of T-cell acute lymphogenic leukemia, the absence of the PEST domain increases the stability of NICD, causing an excessive Notch-signal transduction phenotype (Weng et al., 2004). These data highlight that the C-terminal region of Notch is a regulatory element in Notch protein turnover, but the exact mechanism remains to be elucidated. We hypothesized that the PEST-containing region acts as a binding site for some crucial factors that regulate Notch signaling. To identify such factors, we performed yeast-two-hybrid screening using the Notch1 C-terminal PEST-containing region.

In this study, we identified zinc finger protein 64 (Zfp64) as interacting with the intracellular domain of Notch1, and demonstrated that Zfp64 acts as a coactivator of NICD. Interestingly, *Zfp64* is a downstream target of Runx2 and mediates the myogenic and osteogenic differentiation of C2C12 cells. Possible roles of Zfp64 in mesenchymal cell differentiation are discussed.

Results

Identification of Zfp64 as an NICD-interacting factor

We used the C-terminal PEST-containing region of mouse Notch1 (amino acids 2487-2531) fused to a GAL4 DNA-binding domain as the bait for yeast-two-hybrid screening. Approximately 2×10^6 clones from a mouse embryonic-day-11 cDNA library were screened for interaction with the bait. From about 1000 highly interacting clones, 100 randomly selected clones were sequenced. *Zfp64* was identified as two independent clones of *Zfp64* isoform D.

At least four alternative splicing variants (isoforms A, B, C and D) have been listed in the GenBank database. Isoforms B and C have minor differences relative to isoform A, with deletions of a few amino acids. By contrast, isoform D has a unique C-terminal region that is derived from genomic DNA used only by isoform D. Mouse and human Zfp64 isoform D has 13 C2H2-type zinc-finger motifs, in which high homology is apparent between the regions spanning zinc-finger motifs 2 to 4 and the region spanning the zinc-finger motifs 5 to 7 (Fig. 1). Motifs 4 and 7 (represented as 4' in Fig. 1) of the human Zfp64 isoform D are almost identical, with 93% similarity in the amino acid sequence and 95% similarity in the nucleic acid sequence. Zinc-finger motifs 8 and 9 (represented as 5' and 6' in Fig. 1) of isoform D are highly homologous to zinc-finger motifs 5 and 6 of the other isoforms. This organization suggests that isoform D derived from the ancestral *Zfp64* by genomic duplication. A similar structure is also observed in the mouse Zfp64 isoform D. Interestingly, the Conserved Domain Search algorithm (NCBI, default setting) showed that zinc-finger region 7 to 9 of isoform D (which does not appear in the other isoforms) has substantial structural homology to the SPF1 putative transcriptional-repressor domain that regulates the G2-M transition (COG5189, NCBI). Therefore, the genetic duplication seems to have added to isoform D not only the extra and different sets of zinc-finger motifs, but also a new functional domain for transcriptional regulation. Both of the clones isolated by the yeast-two-hybrid screen were C-terminal fragments that correspond to the isoform-D-specific region. The clone that encodes a Zfp64-isoform-D-specific fragment, spanning the eighth zinc-finger motif of the C-terminus, was chosen for further analysis (hereafter referred to as Zfp-C'). Several other transcription factors were also identified as being highly interacting clones. These included Spt6 and SKIP, both of which have been suggested to form a transcription complex with NICD (Hubbard et al., 1996; Zhou et al., 2000). Most of the other candidate clones were nuclear molecules. However, no factors known to participate in the protein degradation process were isolated.

Zfp64 associates with NICD

To confirm the interaction between Zfp64 and NICD, we performed a yeast-two-hybrid assay using Zfp64 derivatives and the PEST-containing region. The open-reading frame of *Zfp64* isoform D was cloned and ligated into pGADT7, which encodes the GAL4 activation domain. Zfp-C' (the isoform-D-specific C-terminal region), Zfp-N (the N-terminal region shared by all the isoforms) and Zfp-C (the isoform-A, B, C-specific C-terminal region) were also created and ligated into pGADT7. The PEST-containing region interacted with Zfp64, Zfp-C' and Zfp-C but not with Zfp-N (Fig. 2A). Zfp64 showed no interaction with the vector without the insert or with lamin C, which is known to have no specific interaction with most proteins (Fig. 2A). Protein synthesis in yeast was validated by western blot analysis (Fig. 2B). This result suggested that all the isoforms of Zfp64 interact with NICD. In this study, we focused our analysis on the isoform D. We tested the interaction between N-terminal hemagglutinin (HA)-tagged Zfp64 and Myc-tagged PEST proteins using an in-vitro-translation system. Immunoprecipitation and western blot analysis revealed that Zfp64 associates with the PEST-containing region (Fig. 2C). We examined the subcellular localization of Zfp64 by transfecting green fluorescent protein (GFP)-tagged constructs into U2OS cells. GFP-Zfp64 was mainly observed in the nuclei, showing a cellular localization similar to those of GFP-NICD and GFP-CSL (supplementary material Fig. S2A). Western analysis revealed both Zfp64 and NICD in the cytoplasmic and nuclear protein extracts, whereas CSL was mostly detected in the nuclear extract (supplementary material Fig. S2B). The nuclear-to-cytoplasmic protein ratios determined by densitometric analysis demonstrated that the cytoplasmic localization of Zfp64 was greater than that in the nucleus when it was coexpressed with NICD, whereas its nuclear localization was dominant when it was coexpressed with CSL and NICD. More NICD was detected in the nucleus when it was coexpressed with CSL or Zfp64 (supplementary material Fig. S2C). These results imply that Zfp64 colocalizes with NICD in the process of NICD nuclear translocation by CSL. We co-transfected constructs encoding N-terminal FLAG-tagged NICD or NICD lacking the PEST region (NICD-p) together with HA-tagged Zfp64 into HEK293 cells, and performed immunoprecipitation analysis and western blotting. The preliminary experiment, using EDTA-containing buffer for cell lysis and washing, yielded negative results for ZFP64-NICD association. Nonreducing SDS-PAGE yielded a band pattern identical to that observed under reducing conditions (data not shown), suggesting that the tertiary structure of Zfp64 had been disrupted in the lysis buffer and that Zn^{2+} are required for the preservation of its structure. Therefore, we used a lysis buffer without EDTA, with or without Zn^{2+}. In this procedure, Zfp64 was efficiently recovered by the immunoprecipitation of NICD (Fig. 2D). Zfp64 was also recovered by the immunoprecipitation

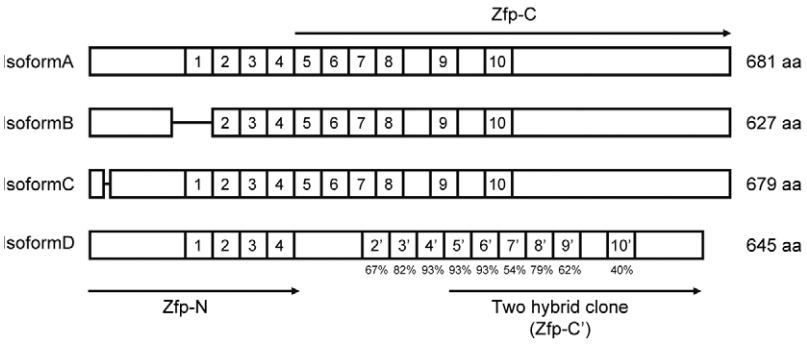

Fig. 1. Illustration of the protein-domain organization of Zfp64. The numbers denote zinc-finger motifs. Zinc-finger motifs 6-9 of isoform-D are highly homologous to the zinc-finger motifs 3-6 of the other isoforms, and are labeled 3', 4', 5', 6' (using the respective numbers). Zinc-finger motifs 5 and 10-13 of isoform-D are labeled 2', 7', 8', 9', 10'. The yeast-two-hybrid screening yielded the isoform-D-specific C-terminal fragment (Zfp-C'). A construct that consists of the region common to all the splicing variants (Zfp-N) and a construct that consists of the C-terminal-fragment specific for isoforms A, B and C (Zfp-C) were created and used in the yeast-two-hybrid assay.

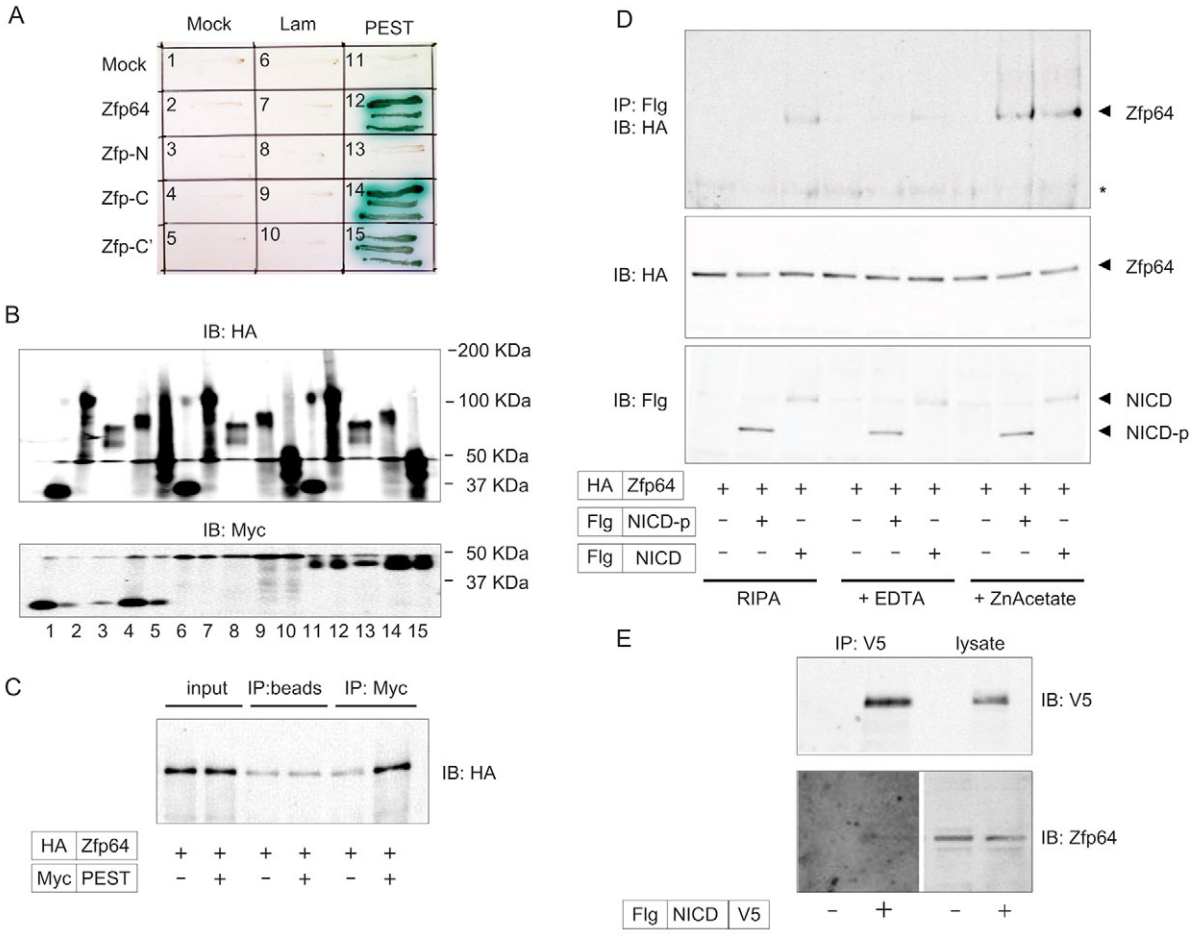

Fig. 2. Zfp64 associates with NICD. (A) Yeast-two-hybrid assay. The PEST-containing region of Notch1 interacts with Zfp64 and its C-terminal region (Zfp-C'), and also with the C-terminal region of the other Zfp64 isoforms (Zfp-C); this was observed by formation of blue colony. Zfp-N, which is the N-terminal region of all the Zfp64 isoforms, showed no interaction with the PEST-containing region. The mock vector and lamin C (Lam) showed no interaction with Zfp64. (B) Translation of the genes fused with a GAL4 activation domain in each yeast transformants was confirmed by Western blot analysis using anti-HA antibody. Translation of the genes fused with a GAL4 DNA-binding domain was confirmed using anti-Myc antibody. (C) Zfp64 associates with the PEST-containing region of Notch1. HA-tagged Zfp64 and Myc-tagged PEST were co-synthesized in vitro using a rabbit reticulocyte lysate system. Immunoprecipitation of the PEST-containing region using anti-Myc antibody revealed co-precipitation of Zfp64. (D) Zfp64 associates with NICD in cells. HA-tagged *Zfp64* and N-terminal FLAG-tagged *NICD* or *NICD-p* were co-transfected into HEK293 cells. Protein extraction and immunoprecipitation were performed in three different lysis buffers: RIPA, RIPA with EDTA, and RIPA with zinc acetate. Immunoprecipitation of NICD using anti-Flag antibody revealed the association of Zfp64 and NICD in RIPA with zinc acetate. A small amount of Zfp64 co-precipitant was detected in RIPA and the least amount of co-precipitant was detected in RIPA with EDTA. Zfp64 also co-precipitated with NICD-p in RIPA with zinc acetate. (E) Endogenous Zfp64 co-precipitated with adenovirally delivered NICD. U2OS cells were transfected with *AdFlg-NICD-V5* and immunoprecipitation with anti-FLAG antibody was performed.

of NICD-p in the buffer with zinc-ion, but not in the buffer without zinc-ion. These results suggest that Zfp64 associates with NICD and that the PEST-containing region is essential for their efficient association, although the region other than the PEST-containing region is also capable of mediating their association. We tried to detect an association between endogenously expressed NICD and Zfp64, but the expression of NICD was insufficient for successful immunoprecipitation, even after coculture with Delta-like-1-expressing HeLa cells (data not shown). Therefore, we overexpressed NICD and examined whether endogenous Zfp64 is co-precipitated with NICD. We used U2OS cells, because the endogenous expression of Zfp64 is relatively high and adenovirus-mediated gene transfer is very efficient in these cells. Endogenous Zfp64 was detected in the precipitant with NICD (Fig. 2E). Collectively, these results indicate that Zfp64 associates with NICD, mainly through the PEST-containing region.

Expression of Zfp64 in tissues and cell lines

We examined the expression of *Zfp64* in tissues and cell lines. Whole-mount in-situ hybridization (ISH) on mouse embryos at 11 days post conception (dpc) revealed that *Zfp64* is expressed in the subepithelial mesenchymal cells, including somites and limb buds (Fig. 3A). ISH using the probe in the sense orientation yielded no significant staining (data not shown). The same expression pattern was observed in a chick embryo at the corresponding developmental stage (HH stage 22), further supporting the validity of the ISH result (Fig. 3B,D). Chick *Hey1* expression is shown for comparison, which was prominent in the somites (Fig. 3C), whereas *Zfp64* was expressed in a broader region of the mesenchymal cells, including the somites. On embryonic day 6 (HH stage 28-29), *Zfp64* expression was prominent in the limb bud, although its expression was ubiquitous in the mesenchyme (Fig. 3E,F). Section ISH on 13.5 dpc mouse embryos revealed that most tissues and organs expressed

Zfp64. Because its expression is almost ubiquitous at this developmental stage, both in epithelial and mesenchymal cells, we show its expression in several representative tissues. In the dermis, *Zfp64* expression was prominent in the dermal basal cells and subepithelial mesenchymal cells (Fig. 3G). *Zfp64* expression was observed in satellite cells, whereas its expression was weak in striated muscles (Fig. 3H). *Zfp64* was expressed in osteoblasts and hypertrophic chondrocytes (Fig. 3I).

Immunohistochemical staining demonstrated the same patterns of expression: the abovementioned cells exhibited distinct nuclear staining (Fig. 3J,K,L). RT-PCR analysis of various organs from an adult mouse revealed ubiquitous expression of *Zfp64* (Fig. 3M). Northern blot analysis confirmed *Zfp64* expression in the brain, spleen, liver, and heart (supplementary material Fig. S3). *Zfp64* expression was detected in diverse mesenchymal cell lines in culture, including fibroblastic (NIH3T3), myogenic (C2C12), chondrogenic (ATDC5), and osteogenic cells (MC3T3-E1, Kusa-A1, U2OS). C2C12 cells showed the strongest expression compared with that in other cell lines, when measured by realtime RT-PCR. *Zfp64* expression was detected in RD-C2 cells established from the calvaria of newborn *Runx2*-knockout mice (Liu et al., 2007) (Fig. 3N). The expression of Zfp64 in C2C12 and U2OS cells was confirmed by immunoblotting and immunocytochemistry (Fig. 3P,Q).

Zfp64 transactivates Notch target genes

To investigate the effect of Zfp64 on Notch signal transduction, we first performed a *Hey1* and *Hes1* promoter assay. *Hes1-luc* or *Hey1-luc* reporter plasmid was co-transfected with *Zfp64* or constitutively active *Notch* constructs into U2OS cells. Zfp64 transactivated both the *Hes1* and *Hey1* promoters in a dose-dependent manner (Fig. 4A,B). The transactivation activity of Zfp64 was comparable with that of the constitutively active Notch constructs (Fig. 4C,D). NICD-p, which lacks the PEST sequence of Notch, showed reduced transactivation activity compared with that of NICD (Fig. 4C,D), but this might not be biologically significant because NICD-p showed higher transactivation activity than NICD at different plasmid concentrations (0.5 μg, data not shown). N-EGF, the

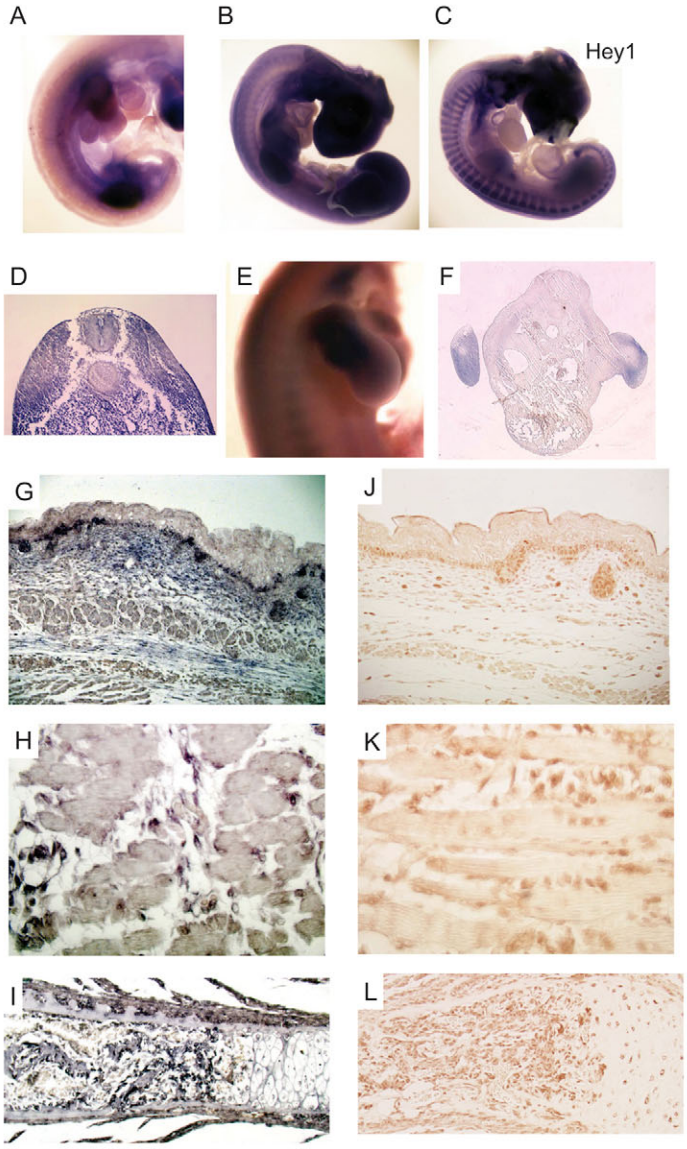

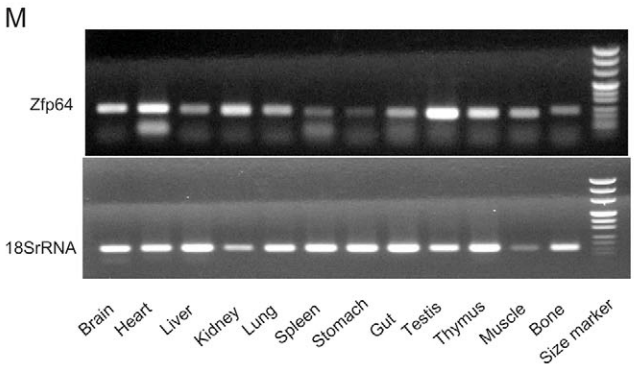

N

Relative expression (xE-03/18SrRNA)

NIH3T3	0.13
ATDC5	0.07
C2C12	5.92
MC3T3-E1	0.30
RD-C2	0.11
U2OS	2.73*

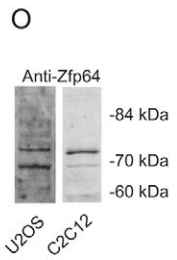

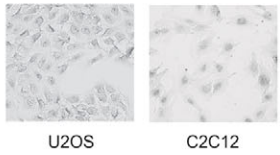

Fig. 3. Zfp64 is expressed in a broad range of mesenchymal tissues. (A,B) Whole-mount in-situ hybridization using a (A) mouse dpc 11 embryo and (B) embryonic day 3.5 (HH stage 22) chick embryo. (C) Chick *Hey1* expression. (D) Section view of B. (E) *Zfp64* expression in an E6 (HH stage 28-29) embryo. (F) Section view of E. (G,H,I) In-situ hybridization to embryonic day 18.5 mouse embryo. *Zfp64* is expressed in (G) the basal layer of the dermis and subepithelial mesenchymal cells, (H) chondrocytes and (I) osteoblasts. (J,K,L) Immunohistochemical staining of an embryonic day 18.5 mouse embryo using anti-Zfp64 antibody shows nuclear staining in an expression pattern similar to that seen in G-I. (M) *Zfp64* expression in adult organs. Ubiquitous expression of *Zfp64* was observed by RT-PCR. (N) *Zfp64* expression in mesenchymal cell lines, measured by real-time PCR. *, Since U2OS cells are a human cell line, the PCR primers were different from those used for the other cell lines. (O) Western blot of C2C12 or U2OS cell lysates using anti-Zfp64 antibody. At least two bands of different molecular mass were observed. The band of the higher molecular mass appears to correspond to isoform A and/or C, and the small protein appears to correspond to isoform B and/or D of Zfp64. (P) Immunocytostaining of C2C12 and U2OS cells using anti-Zfp64 antibody.

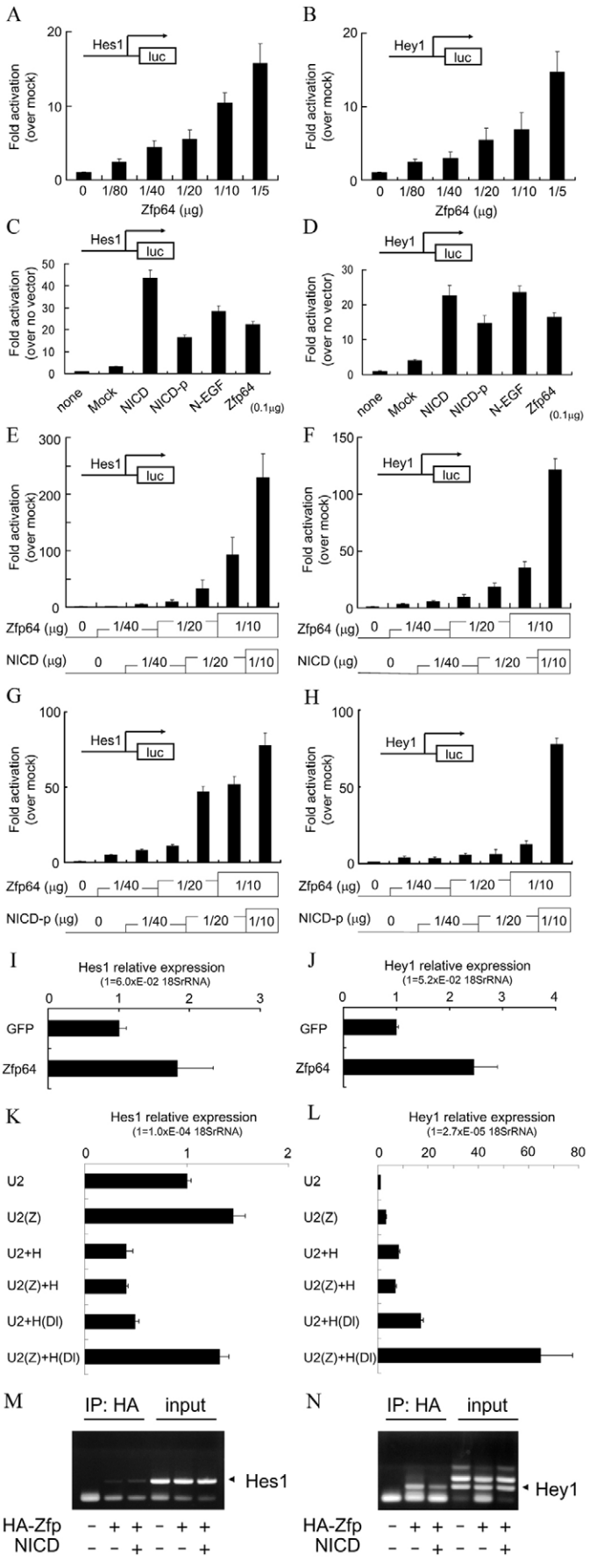

Fig. 4. Zfp64 upregulates *Hes1* and *Hey1* expression. (A,B) Dose-dependent activation of the *Hes1* and *Hey1* promoters by Zfp64. Graded amounts of *Zfp64* plasmid were co-transfected with *Hes1-luc* or *Hey1-luc* reporter plasmids. Data represent the fold-inductions relative to that with mock vector transfection. All the error bars denote standard errors. (C,D) The activation of the *Hes1* or *Hey1* promoter by Zfp64 was similar to the level obtained with constitutively active *Notch* constructs. (E,F) NICD and Zfp64 additively activate the *Hes1* and *Hey1* promoters. Graded amounts of *NICD* and *Zfp64* were co-transfected with the reporter plasmid and the luciferase activity was measured. (G,H) Additive effects of Zfp64 on NICD-p were weak (compare with Fig. 4E,F). (I,J) Zfp64 promoted the expression of *Hes1* and *Hey1*. U2OS cells were transfected with *AdGFP* or *AdZfp64*. Total RNA was extracted 24 hours after infection and real-time RT-PCR analysis was performed. Expression levels of *Hes1* and *Hey1* were normalized to those of 18S rRNA. (K,L) Cells expressing Zfp64 reacted more robustly to Notch signal stimulation with Delta1. U2OS cells were transfected with *AdGFP* (U2) or *AdZfp64* (U2(Z)), co-cultured with one-tenth of the number of HeLa cells (H) or HeLa cells stably transfected with Delta1 (H(Dl)). Real-time PCR analysis was performed after 2 days. Three independently conducted experiments gave similar results and representative data are shown. (M,N) Zfp64 is recruited to the *Hes1* and *Hey1* promoters. HA-tagged *Zfp64* was transfected into U2OS cells with or without *NICD*, and the samples were subjected to a ChIP assay using primers for the *Hes1* or *Hey1* promoter sequence.

membrane-bound form of constitutively active Notch, which lacks all the epidermal growth factor (EGF) repeats but retains the Lin/Notch repeats, also transactivated the *Hes1* and *Hey1* promoters (Fig. 4C,D). When graded amounts of *Zfp64* and *NICD* or *NICD-p* were co-transfected, Zfp64 stimulated the *Hes1* and *Hey1* promoters additively with NICD (Fig. 4E,F), but the additive effects of Zfp64 on NICD-p were weak (Fig. 4G,H).

We measured the mRNA expression of *Hes1* and *Hey1* in U2OS cells following overexpression of *Zfp64*. Real-time RT-PCR 24 hours after adenovirus-*Zfp64* (*AdZfp64*) transfection showed that Zfp64 upregulated *Hes1* and *Hey1* expression twofold compared with that of cells transfected with adenovirus-*GFP* (*AdGFP*) (Fig. 4I,J). Furthermore, co-culture with cells that were constitutively overexpressing Delta1 revealed that cells transfected with *Zfp64* reacted more robustly to Delta1 stimulation than untransfected cells (Fig. 4K,L). Notably, co-culture with cells that do not overexpress Delta1 led to downregulation of *Hes1* and upregulation of *Hey1*. We could not specify the reason for *Hes1* downregulation, but *Hey1* upregulation appears to be owing to endogenous BMP production by HeLa cells, because this cell line is known to secrete substantial amounts of BMPs, and *Hey1* has also emerged as a downstream target of BMP signal transduction, as discussed below. Collectively, these results indicate that Zfp64 promotes Notch signal transfection and upregulates expression of *Hes1* and *Hey1*.

To examine whether this upregulation is caused by the direct binding of Zfp64 to the promoter regions of *Hes1* and *Hey1*, we used chromatin immunoprecipitation (ChIP)-PCR analysis on U2OS cells transfected with the mock or HA-*Zfp64* plasmid using anti-HA antibody. PCR revealed the specific amplification of promoter fragments of *Hes1* and *Hey1* in the HA-*Zfp64*-transfected cells, but not in the mock-transfected cells (Fig. 4M,N). We assumed that co-transfection with *Zfp64* and *NICD* might increase Zfp64 recruitment to the *Hes1* and *Hey1* promoters. However, the ChIP sample of cells co-transfected with *Zfp64* and *NICD* yielded approximately the same or slightly reduced amounts of PCR products. This might be the result of the antagonizing effect of excess amounts of NICD, which captures Zfp64 to form an inefficient transcription complex. We concluded that Zfp64 is recruited to the promoters of *Hes1* or *Hey1*, and that it transactivates these Notch target genes.

Runx2 upregulates Zfp64 expression

Because *Zfp64* has been suggested as a downstream target of Runx2 (Gaikwad et al., 2001), we performed an in silico promoter analysis using the Eldorado software (Genomatix). Eldorado predicted that the core promoter for human *Zfp64* spans from around the –800 position to the transcription initiation site. Two *ose2* Runx2-binding elements were identified in forward and reverse orientations within this region (Fig. 5A). Eldorado also predicted the promoters for mouse and rat *Zfp64*, in both of which a single *ose2* element was identified. The other transcriptional motifs shared by human, mouse, and rat *Zfp64* promoters include *cbf1*- and *hey1*-binding motifs (Fig. 5B). Although the numbers and locations of these motifs differ in the three species, the conservation of these motifs suggests that *Zfp64* expression is under the control of the Runx2 and Notch signaling pathways.

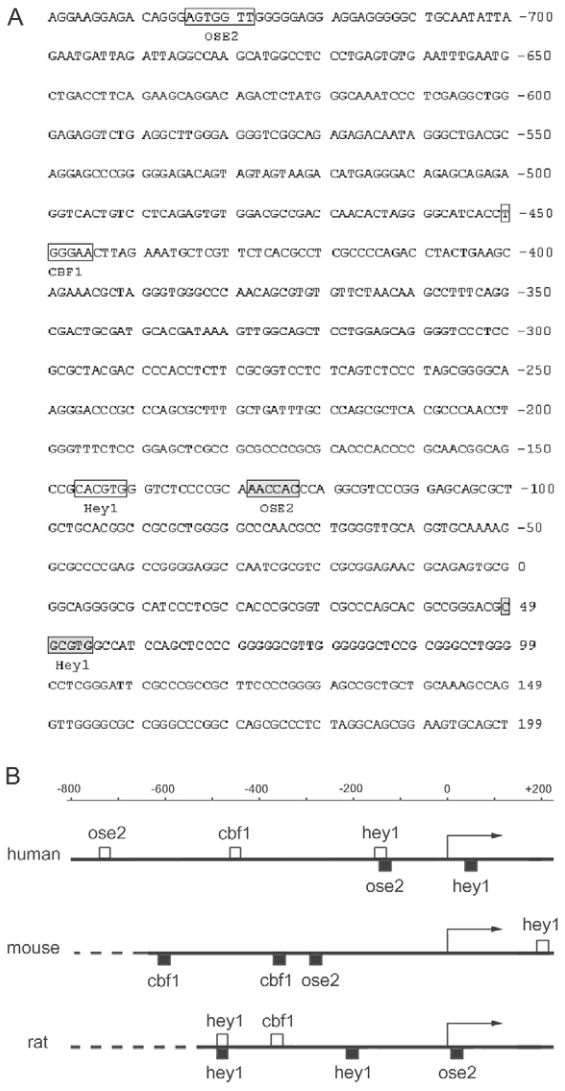

Fig. 5. *Zfp64* promoters. (A) The sequence of the putative promoter of human *Zfp64* and the consensus transcription-factor-binding motifs. White and black squares indicate the core elements in the forward and reverse orientations, respectively. (B) Interspecies comparison of *Zfp64* promoters. The transcription-factor-binding motifs are indicated by white squares (forward orientation) or black squares (reverse orientation).

To explore the regulatory mechanism of *Zfp64* expression, we cloned the putative human *Zfp64* core promoter region and examined its transactivity by luciferase assay. The *Zfp64* promoter was activated by Runx2 in a dose-dependent manner (Fig. 6A). Real-time RT-PCR revealed that *Zfp64* was significantly upregulated 24 hours after adenovirus-*Runx2* (*AdRunx2*) transfection into MC3T3-E1, C2C12 and RD-C2 cells (Fig. 6B).

To investigate the contribution of each *ose2* element to *Zfp64* promoter activity, we created reporter constructs with a deletion or mutation in the *ose2* elements. These reporter plasmids were co-transfected with mock or *Runx2* plasmids and a luciferase assay was performed. *Zfp-luc-m2*, which has a mutation in the proximal *ose2* element, showed Runx2-dependent transactivation, whereas *Zfp-luc-d1* and *Zfp-luc-d2*, which lack the distal *ose2*, as well as *Zfp-luc-m1*, which has a mutation in the distal *ose2*, showed no distinct transactivation by Runx2 (Fig. 6C), suggesting that Runx2 mainly acts on the distal *ose2* element in the human *Zfp64* promoter. These results indicate that Runx2 upregulates *Zfp64* by transactivating the *Zfp64* promoter.

Since Runx2 expression is under the control of BMP signaling and is known to be upregulated by BMP2, we treated MC3T3-E1 cells and RD-C2 cells, both of which were derived from mouse calvarial cells, with 100 ng/ml human recombinant BMP2 protein (rBMP2) and examined the change of expression of *Runx2*, *Zfp64*, *Hes1* and *Hey1*. *Runx2* expression was not altered by BMP2 on day 2, but was upregulated on day 4 in MC3T3-E1 cells (Fig. 6D). The change in *Zfp64* expression was similar to that of *Runx2*; it was unchanged on day 2 and was upregulated on day 4 in MC3T3-E1 cells, whereas *Zfp64* expression was largely unchanged in RD-C2 cells that lack Runx2 expression. *Hey1* expression was upregulated on day 2, prior to *Runx2* and *Zfp64* upregulation, in both cell lines. *Hes1* expression was slightly upregulated on day 2 and day 4, although statistical significance was not confirmed. These results indicate that BMP signaling acts to upregulate *Zfp64* through Runx2 upregulation. *Hes1* upregulation by BMP2 was not prominent, and *Hey1* seems to be a direct target of BMP signaling as well as the Notch signaling, therefore, we could not assess the Runx2-Zfp64-dependent contribution of BMP signaling upon Notch signaling.

Zfp64 is involved in the regulation of mesenchymal cell differentiation

To explore the roles of Zfp64 in myogenic differentiation, we established a C2C12 cell line that carries the *NICD* gene under the control of a tetracycline-inducible promoter. Twelve hours after transduction with *AdGFP* or *AdZfp64*, NICD expression was induced by the addition of doxycycline to the culture medium. Twelve hours after NICD induction, myogenic differentiation was induced by reducing the serum concentration in the culture medium from 20% to 2% (day 0). Doxycycline-induced NICD expression was strongly maintained on day 6, and a substantial level of adenovirally transfected *Zfp64* expression was maintained on day 6 (Fig. 7A), although this expression was attenuated compared with that on day 2. On day 2, the expression of *Mef2C* and *MyoD*, the key myogenic transcription factors, was significantly downregulated in the cells expressing Zfp64 or NICD (Fig. 7C).

Western blot analysis revealed that the expression of sarcomeric actin-α and smooth muscle actin was attenuated in the cells expressing Zfp64 or NICD, and that the cells expressing both Zfp64 and NICD showed a lower level of expression than that of the single-gene-transfected cells (Fig. 7A). The expression of desmin was not

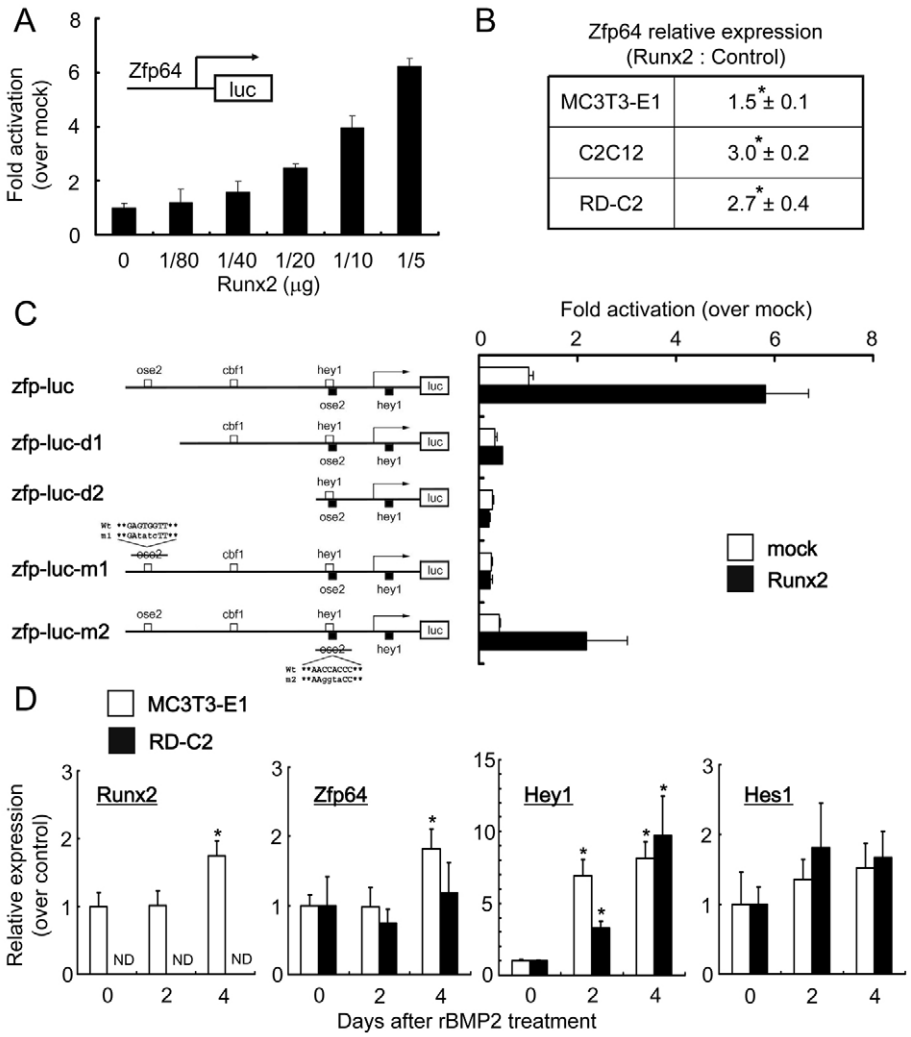

Fig. 6. Runx2 upregulates *Zfp64* expression. (A) Luciferase activity assay. The *Zfp64* promoter was activated by Runx2 in a dose-dependent manner. (B) MC3T3-E1, C2C12, and RD-C2 Runx2-deficient cell lines were transfected with *AdGFP* or *AdRunx2*. *Zfp64* expression was measured by real-time RT-PCR, and shown as Runx2/GFP ratio (means ± s.e.). **P*<0.05. (C) The distal *ose2* element of the human *Zfp64* promoter is crucial for its transactivation by Runx2. Deletions or mutations were introduced into the *Zfp-luc* reporter construct as illustrated, which was co-transfected with the mock or *Runx2* expression plasmid into U2OS cells for a luciferase activity assay. (D) MC3T3-E1 cells or RD-C2 cells were treated with 100 ng/ml of human recombinant BMP2 protein. Expression of *Runx2*, *Zfp64*, *Hey1* and *Hes1* was examined by real-time RT-PCR and was expressed as fold-increase (mean ± s.e.) versus controls without BMP2. **P*<0.05. ND, not detected.

detected in the cells expressing NICD, and was attenuated in the cells expressing Zfp64 (Fig. 7A). C2C12 cells without the overexpression of Zfp64 and NICD generated numerous myotubes. However, myotube formation was significantly inhibited in the cells expressing Zfp64 or NICD (Fig. 7D). The cells overexpressing both Zfp64 and NICD showed the greatest reduction in these muscle-related factors and in myotube formation.

To examine the contribution of endogenous Zfp64 expression to myogenic differentiation, we delivered a small interfering RNA (siRNA) specific for *Zfp64* isoform D, with an adenoviral vector (*AdsiZfp64*). The efficiency of the knockdown effect was confirmed by western blot and real-time PCR analysis (Fig. 7B). Recovery in *Mef2C* and *MyoD* expression were observed in NICD-expressing cells following *AdsiZfp64* transfection (Fig. 7C), although no changes in myotube formation were apparent (Fig. 7D). These results indicate that Zfp64 inhibits myogenic differentiation.

We next investigated the role of Zfp64 in the BMP2-induced osteoblastic differentiation of C2C12 cells. C2C12 cells were treated with a low dose (20 ng/mL) of rBMP2 after 12 hours of transfection using adenovirus vector, and osteogenic markers were examined after 72 hours. Transfection with *AdZfp64* increased the ALP activity of C2C12 cells (Fig. 7E). Conversely, *AdsiZfp64* transfection led to a decrease in ALP activity (Fig. 7E). Transfection with *AdZfp64* upregulated the mRNA for type I collagen (*Col1a1*), osteocalcin (*ocn*), and osteopontin (*opn*), whereas transfection with *AdsiZfp64* caused the downregulation of *col1a1* and *opn* expression (Fig. 7F). These results suggest that Zfp64 positively regulates osteogenic differentiation. In order to examine whether this phenotype is due to Notch signaling activation, we assessed the contribution of Hey1 in the regulation of osteogenic differentiation by Zfp64 using Hey1-deficient calvarial (HDC) cells that had been established from the calvarial cells of a *Hey1*-knockout mouse (Minamizato et al., 2007). We focused on analysis of Hey1 for the following reasons: (1) It is reported to be a regulator of osteogenic differentiation (de Jong et al., 2004; Zamurovic et al., 2004). (2) Zfp64 upregulated *Hey1* more efficiently than *Hes1* in our experiments. The ALP activity of HDC cells was raised by *AdZfp64* transfection and was reduced by *AdHey1* transfection (Fig. 7G), which implicates that the rise in ALP activity by *AdZfp64* transfection is not via Hey1 upregulation. *Col1a1* was upregulated by Hey1, but not by Zfp64 in the HDC cells (Fig. 7H), which implicates that the upregulation of *col1a1* by Zfp64 is the consequence of Hey1 upregulation. Similarly, *opn* expression seems to be mediated by Zfp64, at least in part, through upregulation of Hey1. *Ocn* expression was reduced by *AdHey1* transfection but was not affected by *AdZfp64* in the HDC cells (Fig. 7H). Altogether,

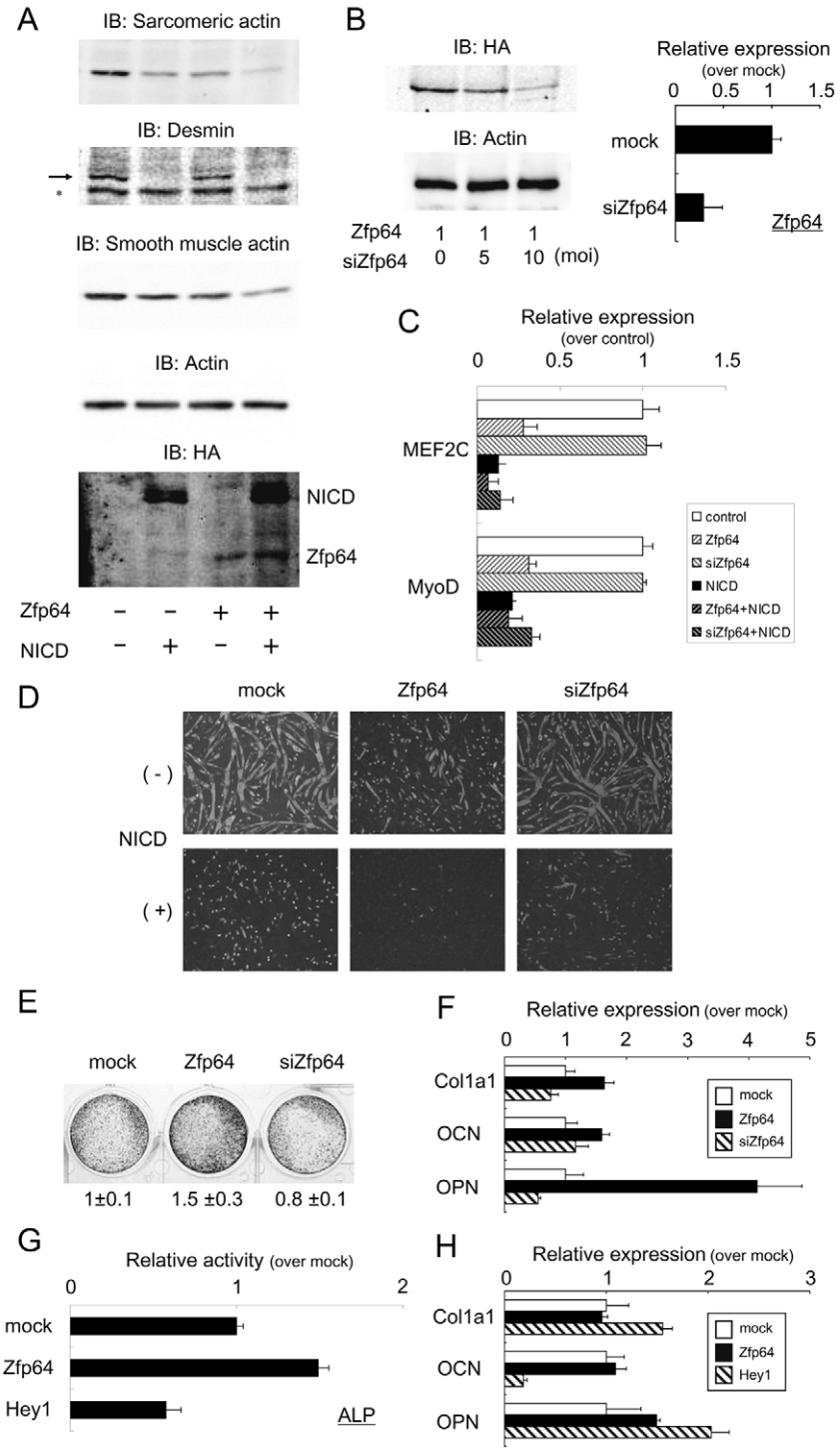

Fig. 7. Zfp64 inhibits myogenesis and promotes the expression of osteogenic marker genes. (A) Zfp64 and NICD inhibit the expression of muscle-specific cytoskeletal proteins. Tet-on-NICD-C2C12 cells were treated as described in Results and western blot analysis was performed. The band specific for desmin is shown by the arrow and the nonspecific band is indicated by an asterisk. (B) siRNA-mediated gene knockdown efficiency. Left. C2C12 cells were co-transfected with *AdZfp64* and *AdsiZfp64* in the indicated ratios. Western blot analysis was performed 1 day after transfection. (Right) C2C12 cells were transfected with mock or *AdsiZfp64*. Real-time PCR was performed 3 days after transfection. (C) Zfp64 and NICD inhibit the expression of myogenic transcription factors. Tet-on-NICD-C2C12 cells were treated as described in Results and real-time RT-PCR was performed. Data shown are representative of two independently conducted experiments (mean ± s.e.). (D) Myotube formation four days after myogenic induction, visualized by immunofluorescent staining using antibody against sarcomeric actin. (E) Alkaline phosphatase (ALP) activity of C2C12 cells increased by Zfp64. C2C12 cells were transfected with *AdGFP*, *AdZfp64* or *AdsiZfp64*. Twelve hours after transfection, cells were treated with 20 ng/ml human recombinant BMP2 protein for 3 days and ALP activity was evaluated. (Top) ALP staining of cells. (Bottom) Relative ALP activity measured using pNPP substrate. Data are expressed as the mean ± s.e. of triplicates. (F) C2C12 cells were treated as described in E, then the expression of type I collagen (*Col1a1*), osteocalcin (*Ocn*) and osteopontin (*Opn*) was examined by real-time RT-PCR. Multiple independently conducted experiments were performed and representative data are shown as the mean ± s.e. of triplicates. (G) Relative ALP activity of HDC cells transfected with *AdGFP*, *AdZfp64* or *AdHey1*. Data are expressed as the mean ± s.e. of triplicates. (H) Relative expression level of *Col1a1*, *Ocn* and *Opn* of HDC cells transfected with *AdGFP*, *AdZfp64* or *AdsiZfp64* (mean ± s.e.).

these results indicate that the effects of Zfp64 on osteogenic differentiation can be attributed partially to Hey1 upregulation, but other mechanisms appear to be involved in the effects of Zfp64.

Discussion

We have demonstrated by yeast-two-hybrid , and in vitro and in vivo binding assays that Zfp64 associates with NICD mainly through the PEST-containing region. The PEST sequences of Notch1 and Notch2 are highly homologous to that of *Drosophila* Notch and are well-conserved beyond these species. By contrast, the PEST sequence of Notch3 shows low similarity to *Drosophila* Notch, and the PEST motif in Notch4 comprises completely different amino acid residues. Considering that the PEST-domain-containing regions of Notch1 and Notch2 have maintained a specific motif against mutation pressure rather than substituting it with other PEST-domain sequences (as seen in Notch3 and Notch4), it is plausible that this motif is used for interactions with some factors that are essential for Notch function.

The primary purpose of our yeast-two-hybrid screen was to identify factors that modify Notch signaling, possibly by regulating Notch protein stabilization or degradation. However, our yeast-two-hybrid experiments yielded no factors related to protein degradation. Instead, several nuclear molecules were isolated as interaction partners. The PEST signal for degradation might be hidden during its interaction with nuclear transcription factors until it is exposed for degradation, after the transcription complex dissociates. This would allow a better control of protein turnover because the protein degradation signal is unmasked in a timely manner to target the protein for degradation.

Zfp64 contains tandem repeats of the C2H2 zinc-finger motifs. A C2H2 zinc finger comprises a pair of cysteine residues in the β-sheet and two histidine residues in the α-helix, which bind Zn^{2+} and interact with the major groove of DNA or RNA. In addition to

its nucleic-acid-binding capacity, a zinc-finger domain can function in protein-protein interactions (Mackay and Crossley, 1998). Because Zn^{2+} is definitely required to stabilize the tertiary structure of the zinc-finger motif, failure to detect the association in the presence of EDTA suggests that metal ions are crucial for maintenance of the correct protein conformation of Zfp64 and its association with NICD. We observed interaction between Zfp64 and NICD-p, although it was weak compared with that between Zfp64 and NICD. This suggests that association with Zfp64 is mediated not just by the PEST-containing region but also by another region. NICD has been proposed to form a dimer through their ankyrin repeats (Nam et al., 2007). However, NICD-p might have associated with endogenous NICD, which, in turn, associates with Zfp64. This might explain the weak association between Zfp64 and NICD-p. Further studies will be required to clarify this point.

The promoter assay and also real-time PCR revealed that Zfp64 upregulates the expression of *Hes1* and *Hey1*, the direct targets of Notch. The effects of Zfp64 on *Hes1* and *Hey1* transcription were additive to those of NICD, but were attenuated in combination with NICD that lacked the PEST-containing region (NICD-p). Furthermore, a ChIP assay showed the recruitment of Zfp64 to the promoters of *Hes1* and *Hey1*. These data suggest that Zfp64 is incorporated into the transcription complex with NICD and contributes to an increase in its transcriptional activity. Therefore, the basic function of Zfp64 might be to strengthen the effects of Notch signaling. It should be noted that our knockdown experiments imply that Zfp64 is not an indispensable factor in Notch signaling. Instead, it might have an additional role in aiding signal transduction.

Gaikwad et al. screened a subtraction library for genes that were significantly downregulated in the tooth germ of *Runx2*-knockout mice, and reported that *Zfp64* is a tooth-specific downstream target of Runx2 (Gaikwad et al., 2001). We showed that the expression of *Zfp64* is under the direct control of Runx2, through the *ose2* elements in the *Zfp64* promoter. This suggests that Runx2 positively acts on Notch signaling through *Zfp64* upregulation. What is the biophysiological significance of this mechanism?

BMP-regulated Runx2 expression has a pivotal role in the transdifferentiation of mesenchymal stem cells. Runx2 regulates the transcription of numerous genes and thereby controls osteoblast development from mesenchymal stem cells (Komori, 2005). Runx2 also suppresses the myogenesis of primary myoblasts and induces their transition to an osteoblastic lineage (Gersbach et al., 2004). Notch signaling exerts a similar effect on myogenesis, by antagonizing MyoD activity and suppressing myoblast differentiation (Kopan et al., 1994; Nofziger et al., 1999). BMP4-mediated inhibition of myoblast differentiation requires functional Notch signaling and seems to coincide with the upregulation of *Hes1* and *Hey1* expression (Dahlqvist et al., 2003). This seems to be achieved without Hes1 activity (Shawber et al., 1996) but the role of another target gene product, Hey1, in blocking myogenesis is yet to be elucidated.

Our data suggest that the upregulation of Zfp64 expression by Runx2 directs cells to follow an osteoblastic lineage rather than a myogenic lineage. Because the synergistic effects of NICD and Zfp64 were observed in our overexpression experiments, the inhibition of myogenic differentiation appears to be achieved, at least partially, through the activation of Notch signal transduction. However, our data also imply a Notch-independent action of Zfp64, and we do not assume that its Notch-dependent action is the only mechanism involving Zfp64 function, considering that Zfp64 exerts its effects in the absence of any forced expression of NICD or Notch signal stimulation. Other interacting partners for Zfp64 have been suggested in a systematic yeast-two-hybrid screening strategy, such as using several nuclear factors, including transducin-like enhancer protein 1/Groucho (Stelzl et al., 2005). The study of other interaction partners might shed light on the Notch-independent functions of Zfp64.

Zfp64 stimulated ALP activity and the mRNA expression of osteogenic marker genes in C2C12 cells. This indicates that Zfp64 is involved in osteoblast differentiation, possibly as a factor downstream from Runx2. Several lines of evidence have demonstrated that Notch signaling is involved in osteoblast differentiation, but the manner in which Notch signaling either inhibits osteoblast differentiation (Deregowski et al., 2006; Sciaudone et al., 2003; Shindo et al., 2003) or promotes it (Nobta et al., 2005; Tezuka et al., 2002) has yet to be elucidated. These multiple effects of Notch signaling have been observed in other cell types, such as blood, skin, and gut epithelium, in which Notch signaling determines binary cell fates or induces terminal differentiation processes, as well as maintains stem cells in a proliferative and pluripotent state (Wilson and Radtke, 2006). These opposing functions appear to be, at least in part, the outcomes of crosstalk with other signaling pathways, such as the Wnt, hedgehog and BMP pathways (Itoh et al., 2004; Wilson and Radtke, 2006).

Both BMP and Notch signaling have crucial roles in the development of various tissues and in the regulation of cell differentiation. Recently, several mechanisms that coordinate the two signaling pathways have been proposed. For example, Smad isoforms form a complex with NICD (Dahlqvist et al., 2003; Sun et al., 2005; Takizawa et al., 2003) in the presence of the coactivators P/CAF and p300, which stabilize the Smad-NICD complexes and promote Notch signal transduction (Itoh et al., 2004; Takizawa et al., 2003). Consequently, Hey1 is synergistically induced by the activation of the Notch and BMP signaling pathways, and Hey1 is thought to be a three-way switch by receiving signals from the Notch and the BMP signaling pathways (Itoh et al., 2004). Another example of BMP and Notch interplay is seen in the downstream transcription factors of the two signaling pathways. Hes1 associates with Runx2 and potentiates Runx2-dependent transcription (McLarren et al., 2000). The association of Hes1 with Runx2 is mediated by the retinoblastoma protein pRb, which further increases Runx2 transactivity in osteoblasts (Lee et al., 2006). We have also reported that the multimodular regulatory protein CCN3/Nov has dual functions that affect both the Notch and BMP signaling pathways. CCN3/Nov interacts with both Notch1 and BMP2, thereby stimulating Notch signal transduction and antagonizing the BMP2 signaling pathway (Minamizato et al., 2007; Sakamoto et al., 2002). In this study, we suggest that Zfp64 is an additional factor that mediates the interplay between the two signaling pathways. The abundant repertoire of mechanisms that coordinate the two signaling pathways should allow for the delicate regulation of the downstream events. This might explain the enigmatic behaviors of the two signaling pathways, which can – depending on the context – act either synergistically or antagonistically.

Materials and Methods

Genes

NICD was generated by PCR from mouse Notch1 cDNA using primers EcoR1-N5353 and N7671-Sal1-Xba1, and was cloned into *Eco*R1-*Sal*1 site of pCMVTag2B (Stratagene). The NICD fragment in pCMVTag2B was digested *Nhe*1-*Sal*1 and ligated into the *Nhe*1-Xho1 site of pcDNA6/V5-HisC (Invitrogen) to create N-terminal FLAG-tagged/C-terminal V5 tagged NICD (Flg-NICD-V5). For NICD without the PEST region, Flg-NICD-V5 was digested with *Nhe*1-*Apa*1 and the insert was ligated

into the *Nhe*1/*Apa*1 site of pcDNA6/V5-HisB(NICD-p). The PEST-containing region (from T2487 to T2517) was obtained by PCR using primers EcoR1-N7450 and N7623-Sal1, and was cloned into the *Eco*R1/*Sal*1 site of pGBKT7(pGBKT7-PEST). cDNA for murine Zfp64 isoform D (Genbank accession number BC004695) was provided by the MRC geneservice (Hinxton, UK). Zfp64 open reading frame was obtained by PCR using primers EcoR1-mZf109 and T7 the plasmid as a template, and was ligated into the *Eco*R1-*Xba*1 site ofHA-pcDNA3 to generate N-terminal HA-tagged Zfp64 (HA-Zfp64, or described as Zfp64). The *Eco*R1-*Sac*1 fragment from HA-Zfp64 was ligated into pGADT7. For Zfp64-N, the primers EcoR1-mZf109 and mZf1327-Sal1 were used for PCR and the amplified fragment was digested with *Eco*R1-*Sal*1 and was ligated into *Eco*R1-*Xho*1 site of pGADT7 (Clontech). Zfp-C was cloned by PCR, and reamplified by PCR using the primers R1-mZf1326 and ligated into *Eco*R1-*Xba*1 site of pGADT7-Rec. N-EGF has been previously described (Sakamoto et al., 2005). For the knockdown experiment, micro RNAi (miRNAi) vector targeting the isoform-D-specific coding region of mZfp64 was created using the BLOCK-iT PolII miR RNAi Expression Vector Kits (Invitrogen). The sequences of pre-miRNA oligonucleotides (miR-Zfp64up and miR-Zfp64down) are given in supplementary material Fig. S1. Mouse CSL cDNA was provided from RIKEN GeneBank courtesy of T. Honjo (Department of Immunology and Genomic Medicine, Kyoto University, Japan). Mouse Hey1 has been previously described (Minamizato et al., 2007). GFP-tagged constructs were created by ligating the PCR-amplified cDNA into pAcGFP1-N1 (Clontech). Runx2 was amplified by primers Nhe1-Rx1 and Rx1791-Sal1 and was ligated into *Nhe*1-*Xho*1 sites of pcDNA6/V5-His. PAC clone RP4-548G19 which contains human Zfp64 geneon chromosome 20 was obtained from the Sanger Institute (Hinxton, UK). The promoter region for human Zfp64 was predicted by ElDorado (Genomatix Software) and was obtained by PCR using primers hgZf51231 and hgZf52118 with PCR solution containing 10% DMSO. The PCR product was cloned into pGL3-basic (Promega; Zfp-luc). The deleted promoter constructs Zfp-luc-d1 and Zfp-luc-d2 were created by *Xho*1-*Hin*dIII or *Sac*1 digestion of Zfp-luc, respectively, and ligated into pGL3-basic. Zfp-luc-m1 and Zfp-luc-m2 were generated by site-directed mutagenesis according to the two-stage amplification protocol (Wang and Malcolm, 1999). All the PCRs, except site-directed mutagenesis which used Pfu turbo (Stratagene), were conducted using BDAdvantage 2 Polymerase Mix (Clontech) and the sequences were verified by DNA sequencing.

Yeast-two-hybrid screening

Yeast-two-hybrid screening was performed using Matchmaker two-hybrid system 3 (Clontech) according to the manufacturer's instructions. AH109 yeast cells were transformed with *pGBKT7-PEST* and were mated with the Y187 cells transformed with mouse 11-day embryo cDNA library (Matchmaker Pretransformed cDNA library, Clontech). Approximately two million diploid cells were spread on SD dropout (-Ade/-His/-Leu/-Trp) plates and incubated. Candidate clones were re-plated on SD drop-out plate with α-X-gal to confirm the bait-prey interactions. The plasmids were extracted from true-positive clones that yielded distinct blue coloration, amplified in *E. coli* and then submitted to DNA sequencing. For confirmation of protein interaction, bait constructs in *pGBKT7* and prey constructs in *pGADT7* were transformed into AH109 and Y187 respectively, and the transformants were cloned and mated together. Mated cultures were spread on SD dropout plates and incubated. *pGBKT7* without an insert and *pGBKT7-Lam*, which contains the gene for human lamin C, were used as negative controls.

Cell culture, transfection, in vitro translation and protein extraction

All cells were cultured in DMEM supplemented with 10% fetal calf serum (FCS) and penicillin-streptomycin, except C2C12 cells were, which were maintained in DMEM with 20% FCS. Transfection was performed using Geneshuttle 40 (Qbiogene) or Fugene 6 (Roche). The cells were lysed 48 hours after transfection with HNTZ buffer (10 mM HEPES pH 7.4, 150 mM NaCl, 1% Triton X-100, 0.02 mM zinc acetate) containing 1× protease inhibitor cocktail (Sigma) or RIPAZ (50 mM Tris pH 8.0, 150 mM NaCl, 1% NP-40, 0.5% sodium deoxycholate, 0.1% SDS, 0.05 mM zinc acetate). For extraction of cytoplasmic protein, HKMZI (10 mM HEPES pH 7.9, 10 mM KCl, 1.5 mM $MgCl_2$, 0.02 mM zinc acetate, 0.6% IGEPAL CA-630 (Sigma) was used, followed by nuclear protein extraction with HNMZG (20 mM HEPES pH 7.9, 420 mM NaCl, 1.5 mM $MgCl_2$, 0.05 mM zinc acetate, 25% glycerol). In vitro transcription and translation were performed using a TNT T7-coupled reticulocyte lysate system (Promega).

Immunoprecipitation and western blot analysis

Immunoprecipitation was conducted using anti-FLAG M2 affinity gel (Sigma), Profound Myc tag IP/Co-IP Kit (Pierce) or anti-V5 agarose (GeneTex) for 1 hour or overnight at 4°C. The beads were washed four times with RIPAZ buffer. SDS-PAGE was performed using 1× sample buffer containing 10% β-mercaptoethanol. The proteins were transferred to the nitrocellulose membrane (Hybond-ECL, Amersham). Nonspecific binding was blocked with 2% blocking solution (Amersham) in TBST (10 mM Tris pH 7.6, 150 mM NaCl, 0.1% Tween 20) and incubated with an antibody for 1 hour or overnight. The membranes were washed four times with TBST each for 5 minutes. For the antibodies that have not been coupled to peroxidase, incubation with secondary antibody was conducted. Chemiluminescent detection was performed using an ECL Advance Chemiluminescence Detection Kit (Amersham). The following antibodies were used in this study: anti-Zfp64 (Orbigen), anti-actin (SC-8432, Santa Cruz), anti-sarcomeric-actin-α (clone 5C5, Sigma), anti-desmin (CloneD33, DAKO), anti-α-smooth muscle actin (Clone 1A4, DAKO), anti-HA (clone 3F10, Roche), anti-Flag M2 (Sigma), anti-Myc (Clontech) and anti-V5 (Invitrogen) antibodies.

In-situ hybridization and immunohistochemistry

Whole-mount in situ hybridization was performed as previously described (Sakamoto et al., 1998). For section-mount in-situ hybridization, embryos were fixed in 4% paraformaldehyde-PBS for 24 hours, decalcified in 10% EDTA at 4°C for one week, embedded in paraffin and sectioned 4 μm thick. For mouse *Zfp64*, the open reading frame was used as a template for the digoxygenin-labeled RNA probe. For chick *Zfp64* and *Hey1*, cDNA fragments for RNA probe templates were PCR amplified using the primer sets cZf2020/cZf2573 and cHy709/cHy1081. Immunohistochemical staining was performed on formalin-fixed, EDTA-decalcified and paraffin-embedded sections. Epitope retrieval was performed in 10 mM Tris (pH 9.0) supplemented with 1 mM EDTA for 20 minutes at 120°C in an autoclave machine. Endogenous peroxidase activity was killed in 10% hydrogen peroxidase/methanol and nonspecific binding was blocked in 10% horse serum/TBST. Incubation with anti-Zfp64 antibody was done overnight at 4°C. After washing, the sections were incubated with biotin-conjugated anti-IgY antibody (Abcam) and then with peroxidase-conjugated streptavidin. The antigen-bound peroxidase activity was visualized with diaminobenzidine substrate.

Northern blot analysis, RT-PCR and real-time PCR

Total RNA was extracted using a NucleoSpin RNA II Kit (Macherey-Nagel). Northern blot analysis was performed using a digoxygenin-labeled RNA probe according to the DIG Application Manual for Filter Hybridization (Roche). Total RNA was reverse transcribed using oligo-dT primer and real-time PCR was performed using a LightCycler ST300 system (Roche) with a Platinum SYBR Green qPCR SuperMix UDG Kit (Invitrogen). Primers used for the real-time PCR are listed in the supplementary material Fig. S1. Expression levels of each gene were normalized to *18S rRNA* expression using delta-delta Ct method.

Recombinant adenovirus production and infection

HA-Zfp64 and the *miRNA-Zfp64* knockdown construct were cloned into *pDNR-CMV* (Clontech) and were recombined by Cre recombinase into *pLP-AdenoX* (Clontech). Adenovirus production was carried out according to the manufacturer's instruction. Adenovirus GFP (*AdGFP*) and adenovirus Runx2 (*AdRunx2*) have been previously described (Hirata et al., 2003). The viral titers of *AdZfp64* were evaluated in HEK293 cells by immunocytostaining using anti-Hexon antibody (Clontech). Adenovirus transduction was done at multiplicity of infection (MOI) of 50 in HEK293. Using *AdGFP*, we confirmed that MOI 50 is sufficient to achieve virtually 100% infection of C2C12 cells.

Luciferase-activity assay

The *Zfp64-luc* reporter vector and its derivatives were created as described above (Genes section). The original *HES1* promoter fragment was a gift from R. Kageyama (Institute for Virus Research, Kyoto University, Japan) and has been described previously (Sakamoto et al., 2002). *Hey1-luc* was kindly provided by M. Gessler (Biocenter, University of Würzburg, Germany). The total amounts of the plasmids for transfection were equalized to 0.3 μg by adding the mock plasmid. Transfections were done into U2OS cells on 48 well plates and the luciferase activity was measured 48 hours after transfection. All transfections were carried out in triplicate and the experiments were repeated at least twice. Statistical analysis was performed using Excel 2003 (Microsoft).

Chromatin immunoprecipitation (ChIP) assay

U2OS cells were spread on 24-well plates and were transfected with *Zfp64* or/and *NICD*. ChIP assay was performed basically according to the protocol provided by Abcam (available online at http://www.abcam.com/ps/pdf/protocols/x_chip_protocol.pdf.). In brief, cells were fixed in 1% formaldehyde for 15 minutes at room temperature. Fixation was terminated by adding glycine to 0.13 M and washing twice in PBS. After cell lysis, DNA was sheared by carrying out a 20-second sonication five times (power gauge 6, Handy Sonic UR-20P, Tomy Seiko, Japan). The lysates were immunoprecipitated using anti-HA affinity matrix (Roche) and washed thoroughly. Samples were de-crosslinked at 65°C and after RNase and proteinase K treatments, the immunoprecipitated DNA fragments were purified by phenol/chloroform extraction and ethanol precipitation. The presence of promoter fragment was evaluated by PCR. The PCR conditions were 34 cycles of 94°C for 30 seconds, 59°C for 30 seconds, 72°C for 30 seconds, The PCR primer sets hgHs521/hgHs747 and hgHy519/hgHy686 were used for detection of *Hes1* and *Hey1* promoter fragments, respectively.

Immuocytostaining

For myotube staining, cells were fixed with methanol for 5 minutes, blocked in TBST supplemented with 10% horse serum for 10 minutes and incubated with mouse antibody against sarcomeric actin (clone 5C5, Sigma, dilution 1:200) for 30 minutes. After washing, the cells were incubated with Alexa-Fluor-488-conjugated goat anti-

mouse IgG (Molecular Probes, dilution 1:500) and DAPI Solution (Dojindo, Japan, dilution 1:10,000) for 10 minutes. After brief washing, cells were visualized under a fluorescent microscope (Axioscop2, Zeiss). For Zfp64 staining, cells were fixed with PBS supplemented with 4% paraformaldehyde and endogenous peroxidase activity was quenched by 10% hydrogen peroxidase. Peroxidase-conjugated anti-IgY antibody (Chemicon) was used as a secondary antibody.

Alkaline phosphatase (ALP) staining and ALP-activity assay

Cells were fixed with methanol for 5 minutes and stained in NBT/BCIP substrate (Roche). For colorimetric assay, cells were lysed with HNT buffer (10 mM HEPES pH 7.4, 150 mM NaCl, 1% Triton X-100) and 10 µl of the lysate was incubated with 100 µl of *p*-nitrophenyl phosphate solution (Wako Chemical, Japan) at 37°C for 1 hour and absorbance at 405 nm was measured. The values were normalized to the protein concentrations.

This work has been supported by Grant-in-Aid for Scientific Research to K.S. and A.Y. from the Ministry of Education, Science, Sports and Culture.

References

Dahlqvist, C., Blokzijl, A., Chapman, G., Falk, A., Dannaeus, K., Ibanez, C. F. and Lendahl, U. (2003). Functional Notch signaling is required for BMP4-induced inhibition of myogenic differentiation. *Development* **130**, 6089-6099.

de Jong, D. S., Vaes, B. L., Dechering, K. J., Feijen, A., Hendriks, J. M., Wehrens, R., Mummery, C. L., van Zoelen, E. J., Olijve, W. and Steegenga, W. T. (2004). Identification of novel regulators associated with early-phase osteoblast differentiation. *J. Bone Miner. Res.* **19**, 947-958.

Deregowski, V., Gazzerro, E., Priest, L., Rydziel, S. and Canalis, E. (2006). Notch 1 overexpression inhibits osteoblastogenesis by suppressing Wnt/beta-catenin but not bone morphogenetic protein signaling. *J. Biol. Chem.* **281**, 6203-6210.

Ducy, P. (2000). Cbfa1: a molecular switch in osteoblast biology. *Dev. Dyn.* **219**, 461-471.

Ehebauer, M., Hayward, P. and Martinez-Arias, A. (2006). Notch signaling pathway. *Sci. STKE* **2006**, cm7.

Fryer, C. J., White, J. B. and Jones, K. A. (2004). Mastermind recruits CycC:CDK8 to phosphorylate the Notch ICD and coordinate activation with turnover. *Mol. Cell* **16**, 509-520.

Gaikwad, J. S., Cavender, A. and D'Souza, R. N. (2001). Identification of tooth-specific downstream targets of Runx2. *Gene* **279**, 91-97.

Gersbach, C. A., Byers, B. A., Pavlath, G. K. and Garcia, A. J. (2004). Runx2/Cbfa1 stimulates transdifferentiation of primary skeletal myoblasts into a mineralizing osteoblastic phenotype. *Exp. Cell Res.* **300**, 406-417.

Gupta-Rossi, N., Le Bail, O., Gonen, H., Brou, C., Logeat, F., Six, E., Ciechanover, A. and Israel, A. (2001). Functional interaction between SEL-10, an F-box protein, and the nuclear form of activated Notch1 receptor. *J. Biol. Chem.* **276**, 34371-34378.

Hirata, K., Tsukazaki, T., Kadowaki, A., Furukawa, K., Shibata, Y., Moriishi, T., Okubo, Y., Bessho, K., Komori, T., Mizuno, A. et al. (2003). Transplantation of skin fibroblasts expressing BMP-2 promotes bone repair more effectively than those expressing Runx2. *Bone* **32**, 502-512.

Hubbard, E. J., Dong, Q. and Greenwald, I. (1996). Evidence for physical and functional association between EMB-5 and LIN-12 in Caenorhabditis elegans. *Science* **273**, 112-115.

Itoh, F., Itoh, S., Goumans, M. J., Valdimarsdottir, G., Iso, T., Dotto, G. P., Hamamori, Y., Kedes, L., Kato, M. and ten Dijke, P. (2004). Synergy and antagonism between Notch and BMP receptor signaling pathways in endothelial cells. *EMBO J.* **23**, 541-551.

Katagiri, T., Yamaguchi, A., Komaki, M., Abe, E., Takahashi, N., Ikeda, T., Rosen, V., Wozney, J. M., Fujisawa-Sehara, A. and Suda, T. (1994). Bone morphogenetic protein-2 converts the differentiation pathway of C2C12 myoblasts into the osteoblast lineage. *J. Cell Biol.* **127**, 1755-1766.

Komori, T. (2005). Regulation of skeletal development by the Runx family of transcription factors. *J. Cell. Biochem.* **95**, 445-453.

Kopan, R., Nye, J. S. and Weintraub, H. (1994). The intracellular domain of mouse Notch: a constitutively activated repressor of myogenesis directed at the basic helix-loop-helix region of MyoD. *Development* **120**, 2385-2396.

Lee, J. S., Thomas, D. M., Gutierrez, G., Carty, S. A., Yanagawa, S. and Hinds, P. W. (2006). HES1 cooperates with pRb to activate RUNX2-dependent transcription. *J. Bone Miner. Res.* **21**, 921-933.

Liu, T., Gao, Y., Sakamoto, K., Minamizato, T., Furukawa, K., Tsukazaki, T., Shibata, Y., Bessho, K., Komori, T. and Yamaguchi, A. (2007). BMP-2 promotes differentiation of osteoblasts and chondroblasts in Runx2-deficient cell lines. *J. Cell. Physiol.* **211**, 728-735.

Mackay, J. P. and Crossley, M. (1998). Zinc fingers are sticking together. *Trends Biochem. Sci.* **23**, 1-4.

Matsuno, K., Eastman, D., Mitsiades, T., Quinn, A. M., Carcanciu, M. L., Ordentlich, P., Kadesch, T. and Artavanis-Tsakonas, S. (1998). Human deltex is a conserved regulator of Notch signalling. *Nat. Genet.* **19**, 74-78.

McLarren, K. W., Lo, R., Grbavec, D., Thirunavukkarasu, K., Karsenty, G. and Stifani, S. (2000). The mammalian basic helix loop helix protein HES-1 binds to and modulates the transactivating function of the runt-related factor Cbfa1. *J. Biol. Chem.* **275**, 530-538.

Minamizato, T., Sakamoto, K., Liu, T., Kokubo, H., Katsube, K. I., Perbal, B., Nakamura, S. and Yamaguchi, A. (2007). CCN3/NOV inhibits BMP-2-induced osteoblast differentiation by interacting with BMP and Notch signaling pathways. *Biochem. Biophys. Res. Commun.* **354**, 567-573.

Nam, Y., Weng, A. P., Aster, J. C. and Blacklow, S. C. (2003). Structural requirements for assembly of the CSL.intracellular Notch1.Mastermind-like 1 transcriptional activation complex. *J. Biol. Chem.* **278**, 21232-21239.

Nam, Y., Sliz, P., Pear, W. S., Aster, J. C. and Blacklow, S. C. (2007). Cooperative assembly of higher-order Notch complexes functions as a switch to induce transcription. *Proc. Natl. Acad. Sci. USA* **104**, 2103-2108.

Nobta, M., Tsukazaki, T., Shibata, Y., Xin, C., Moriishi, T., Sakano, S., Shindo, H. and Yamaguchi, A. (2005). Critical regulation of bone morphogenetic protein-induced osteoblastic differentiation by Delta1/Jagged1-activated Notch1 signaling. *J. Biol. Chem.* **280**, 15842-15848.

Nofziger, D., Miyamoto, A., Lyons, K. M. and Weinmaster, G. (1999). Notch signaling imposes two distinct blocks in the differentiation of C2C12 myoblasts. *Development* **126**, 1689-1702.

Oberg, C., Li, J., Pauley, A., Wolf, E., Gurney, M. and Lendahl, U. (2001). The Notch intracellular domain is ubiquitinated and negatively regulated by the mammalian Sel-10 homolog. *J. Biol. Chem.* **276**, 35847-35853.

Sakamoto, K., Nakamura, H., Takagi, M., Takeda, S. and Katsube, K. (1998). Ectopic expression of lunatic Fringe leads to downregulation of Serrate-1 in the developing chick neural tube; analysis using in ovo electroporation transfection technique. *FEBS Lett.* **426**, 337-341.

Sakamoto, K., Yamaguchi, S., Ando, R., Miyawaki, A., Kabasawa, Y., Takagi, M., Li, C. L., Perbal, B. and Katsube, K. (2002). The nephroblastoma overexpressed gene (NOV/ccn3) protein associates with Notch1 extracellular domain and inhibits myoblast differentiation via Notch signaling pathway. *J. Biol. Chem.* **277**, 29399-29405.

Sakamoto, K., Chao, W. S., Katsube, K. and Yamaguchi, A. (2005). Distinct roles of EGF repeats for the Notch signaling system. *Exp. Cell Res.* **302**, 281-291.

Sciaudone, M., Gazzerro, E., Priest, L., Delany, A. M. and Canalis, E. (2003). Notch 1 impairs osteoblastic cell differentiation. *Endocrinology* **144**, 5631-5639.

Shawber, C., Nofziger, D., Hsieh, J. J., Lindsell, C., Bogler, O., Hayward, D. and Weinmaster, G. (1996). Notch signaling inhibits muscle cell differentiation through a CBF1-independent pathway. *Development* **122**, 3765-3773.

Shindo, K., Kawashima, N., Sakamoto, K., Yamaguchi, A., Umezawa, A., Takagi, M., Katsube, K. and Suda, H. (2003). Osteogenic differentiation of the mesenchymal progenitor cells, Kusa is suppressed by Notch signaling. *Exp. Cell Res.* **290**, 370-380.

Stelzl, U., Worm, U., Lalowski, M., Haenig, C., Brembeck, F. H., Goehler, H., Stroedicke, M., Zenkner, M., Schoenherr, A., Koeppen, S. et al. (2005). A human protein-protein interaction network: a resource for annotating the proteome. *Cell* **122**, 957-968.

Sun, Y., Lowther, W., Kato, K., Bianco, C., Kenney, N., Strizzi, L., Raafat, D., Hirota, M., Khan, N. I., Bargo, S. et al. (2005). Notch4 intracellular domain binding to Smad3 and inhibition of the TGF-beta signaling. *Oncogene* **24**, 5365-5374.

Takizawa, T., Ochiai, W., Nakashima, K. and Taga, T. (2003). Enhanced gene activation by Notch and BMP signaling cross-talk. *Nucleic Acids Res.* **31**, 5723-5731.

Tezuka, K., Yasuda, M., Watanabe, N., Morimura, N., Kuroda, K., Miyatani, S. and Hozumi, N. (2002). Stimulation of osteoblastic cell differentiation by Notch. *J. Bone Miner. Res.* **17**, 231-239.

Wang, W. and Malcolm, B. A. (1999). Two-stage PCR protocol allowing introduction of multiple mutations, deletions and insertions using QuikChange Site-Directed Mutagenesis. *Biotechniques* **26**, 680-682.

Weng, A. P., Ferrando, A. A., Lee, W., Morris, J. P., 4th, Silverman, L. B., Sanchez-Irizarry, C., Blacklow, S. C., Look, A. T. and Aster, J. C. (2004). Activating mutations of NOTCH1 in human T cell acute lymphoblastic leukemia. *Science* **306**, 269-271.

Wilson, A. and Radtke, F. (2006). Multiple functions of Notch signaling in self-renewing organs and cancer. *FEBS Lett.* **580**, 2860-2868.

Wu, G., Lyapina, S., Das, I., Li, J., Gurney, M., Pauley, A., Chui, I., Deshaies, R. J. and Kitajewski, J. (2001). SEL-10 is an inhibitor of notch signaling that targets notch for ubiquitin-mediated protein degradation. *Mol. Cell. Biol.* **21**, 7403-7415.

Zamurovic, N., Cappellen, D., Rohner, D. and Susa, M. (2004). Coordinated activation of notch, Wnt, and transforming growth factor-beta signaling pathways in bone morphogenic protein 2-induced osteogenesis. Notch target gene Hey1 inhibits mineralization and Runx2 transcriptional activity. *J. Biol. Chem.* **279**, 37704-37715.

Zhou, S., Fujimuro, M., Hsieh, J. J., Chen, L., Miyamoto, A., Weinmaster, G. and Hayward, S. D. (2000). SKIP, a CBF1-associated protein, interacts with the ankyrin repeat domain of NotchIC To facilitate NotchIC function. *Mol. Cell. Biol.* **20**, 2400-2410.